### **CONFERENCE PRE-PRINT**

# Investigation of transient transport dynamics induced by compact torus injection in the EAST tokamak

Zhihao Zhao

Hefei University of Technology/Institute of Energy, Hefei Comprehensive National Science Center

Hefei, China

Email: 1355683029@qq.com

Chengming Qu Institute of Energy, Hefei Comprehensive National Science Center Hefei, China Email: qucm@ie.ah.cn

Zhou Chu University of Science and Technology of China Hefei, China Email: zhouchu@ustc.edu.cn

#### **Abstract**

The rapid rise in plasma core electron temperature triggered by cold plasma injection has long been recognized as a robust demonstration of nonlocal transport. This study reports on experiments investigating nonlocal heat transport via compact torus (CT) injection in the plasmas of the EAST tokamak. In low-density plasmas, the core temperature increases concomitantly with the drop in edge temperature following compact torus injection. Leveraging the inherent properties of compact torus—high density, high velocity, and self-organization, rapid penetration into deeper plasma regions was experimentally achieved. In this experiment, the evolution of plasma electron density during compact torus injection was measured using a high-time-resolution density profile reflectometry diagnostic. The evolution characteristics of electron density show that after CT injection, the electron density in the plasma core rises rapidly, which quickly flattens the plasma density profile. Meanwhile, internal plasma turbulence plays a crucial role in mediating nonlocal transport phenomena. Using Doppler Backscattering (DBS) diagnostics, we observed quasi-coherent trapped electron modes (QC-TEM) and found that their intensity decreases significantly following CT injection. The simulation results based on the Trapped Gyro-Landau Fluid (TGLF) transport model are consistent with the experimental results. The plasma core temperature response can indeed be attributed to the stabilization of Trapped Electron Mode (TEM) turbulence induced by the reduction in the electron density gradient. Both simulation and experimental results demonstrate that the local transport model can well explain the core temperature increase induced by cold pulse injection.

#### 1. INTRODUCTION

Understanding the transport mechanisms in magnetically confined plasmas is critical for advancing nuclear fusion research, and mastering the dynamics of transient plasmas is equally indispensable for controlling future fusion reactors [1]. The experiments conducted in the TEXT tokamak in 1995 demonstrated that adding a perturbed cold pulse at the low collision plasma boundary led to a decrease in the boundary temperature while the core temperature rose rapidly [2]. Subsequently, this phenomenon was reported in multiple tokamaks and stellarators (TFTR [3], Tore Supra [4], ASDEX-U [5], JET [6], HL-2A [7], EAST [8], Alcator C-Mod [9], KSTAR [10], J-TEXT [11], LHD [12] and RTP [13]). The decrease in boundary temperature was caused by the energy exchange resulting from the injection of neutral particles. However, the rapid response of the core temperature (much faster than the energy confinement time) and its subsequent increase remain poorly explained.

In early studies, various type of empirical models, marginal stability models, and self-organized criticality models were developed to explain the nonlocal phenomenon. Subsequent experiments on JET utilized nonlocal models based on fractional diffusion [14] operators to describe nonlocal phenomena. At the same time, models based on turbulence spreading [15] and residual stresses were proposed to reconstruct the nonlocal phenomena. Furthermore, measurements conducted on EAST following supersonic molecular beam injection (SMBI) have revealed results concerning plasma electron temperature, density, and density fluctuations during the non-local phase. Experimental results from the Alcator C-Mod device, combined with modeling studies based on TGLF, provided a qualitative explanation for the core temperature reversal phenomenon [16]. This is believed to result from the stabilization of TEM turbulence, induced by the abrupt flattening of the electron density profile caused

by impurity ablation injection. However, in Alcator C-Mod the evolution of the electron density profiles was not experimentally measured with high temporal resolution. The electron density distribution used in the simulation was constructed as a Gaussian distribution with an inward-propagating skewness. Subsequent identical impurity injection experiments on DIII-D [17], which combined density evolution data from high-resolution reflectometry with the model, successfully reconstructed the temperature reversal phenomenon. In ASDEX Upgrade [18], further studies supplemented results from laser impurity injection experiments combined with TGLF simulations under different heating conditions: a rapid increase in central electron temperature occurs exclusively in plasmas with electron-dominated heating, whereas such a rapid increase is not observed in plasmas with ion-dominated heating. These results further confirm that local transport model can reproduce the temperature reversal phenomenon.

Two key issues arise from the temperature inversion following cold pulse injection: (1) the core electron temperature increase and (2) the rapidity of core electron temperature change. The core electron temperature rise has been explained by the competition between TEM and ITG modes, but the mechanism underlying the extremely rapid core electron temperature change remains poorly validated. In previous nonlocal experiments on EAST triggered by SMBI, turbulence was observed to play a crucial role in nonlocal phenomena. However, the density only began to respond approximately 10 milliseconds after SMBI. Compared with SMBI, CT injection can rapidly deposit into deeper plasma regions due to its inherent characteristics of high velocity and high density. Building on existing theories and incorporating the rapid core penetration achieved by CT injection along with the accompanying density changes, investigations into non-local phenomena can help further elucidate the mechanisms underlying ultrafast core temperature reversal.

The remainder of this paper is organized as follows. Section 2 describes the experimental setup for CT injection induced nonlocal phenomena, including the CT injection system configuration, heating methods, diagnostic arrangements, and relevant plasma parameters. The primary experimental results are presented in Section 3, encompassing electron temperature responses to CT injection under high and low plasma density scenarios, density evolution at different radial positions, and the evolution of density and temperature profiles. Linear stability analysis using the Trapped Gyro-Landau-Fluid transport (TGLF) model is presented in Section 4. Section 5 summarizes the results and discusses future directions.

# 2. EXPERIMENTAL SETUP

EAST is a fully superconducting tokamak device featuring a noncircular poloidal cross-section [19]. It has major radius R = 1.7 - 1.9 m, minor radius a = 0.4 - 0.45 m, maximum magnetic field of 3.5 T, plasma current of 1 MA, flexible double null or single null plasma geometry, and an ITER-like configuration. The experimental results reported in this paper were obtained from a series of plasma discharge experiments on the EAST tokamak. These experiments aimed to investigate the rapid response of plasma to cold pulses through fast compact torus (CT) injection under specific density conditions. These experiments were conducted under the plasma current of  $Ip = 400 \ kA$ , the toroidal magnetic field  $BT = 2.5 \ T$ , a safety factor at the 95% of the toroidal flux q95 = 6.9 and with ECRH heated plasmas.

Figure 1(a) shows the top view of the CT injection system used in this experiment. The CT system was installed on the H window of EAST and connected to EAST through a 100 mm flange opening port positioned 195 mm below the mid-plane [20]. As shown in Figure 1(b), this is the cross-section view of the CT injection system and the essential diagnostics. Due to space constraints, a 1300 mm drift tube installed in the Duva region to guide the CT plasma toward the first wall on the low-field side. To investigate the impact of CT injection on non-local transport processes, high-time-resolution diagnostics were employed to measure the plasma evolution following CT injection. The electron temperature is measured by the electron cyclotron emission radiometer (ECE) [21]. And the evolution process of the density after CT injection can be measured using the reflectometers (REFL) [22] and the polarimeter interferometer (POINT) [23]. Additionally, the multi-channel Doppler backscattering (DBS) system [24-26] measures the electron density fluctuation and perpendicular velocity.

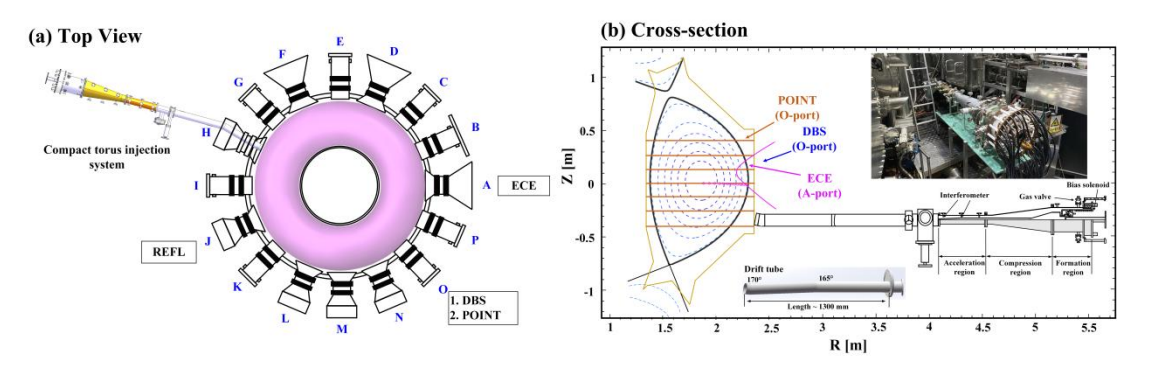


FIG. 1. (a) The schematic top view of CT injection system and essential diagnostics on EAST, such as ECE, DBS, REFL and POINT. (b) The cross-section of CT injection system on EAST. The pink hollow circles indicate the measurement positions of ECE, the blue dash line is the trajectory of the DBS ray, the orange horizontal line is the measurement position of POINT.

### 3. EXPERIMENTAL RESULTS

### 3.1 CHARACTERISTICS OF THE COMPACT TORUS INJECTION SYSTEM ON EAST

Constructing a CT on the EAST aims to achieve central fueling—a crucial objective, as CT fueling has not yet been implemented on a device with such a high magnetic field. This effort can enhance the tritium burn-up rate, which is a key enabler for tritium breeding rate (TBR) and essential for achieving fuel self-sufficiency in future fusion reactors, including the China Fusion Engineering Test Reactor (CFETR). To meet the central fueling requirements of EAST, the EAST CT system exhibits the following characteristics: it can perform 2 Hz repetitive injection [27] and features a wide injection window. At an acceleration bank voltage of 15 kV, the CT kinetic energy density reaches 1300 kJ/m³ [28]. The typical waveforms of CT plasma parameters under 2.4 T background magnetic field of EAST are shown in figure 2(b). The entire discharge process from CT formation to acceleration and ejection is completed within hundreds of microseconds. The CT average plasma density is approximately  $2.1 \times 10^{22} \,\mathrm{m}^{-3}$ , with velocity of CT is approximately  $170 \,\mathrm{km/s}$ . The particle number at CT ejection is about  $1.9 \times 10^{20}$  (corresponding to a mass of 0.64 mg), with a corresponding kinetic energy density of approximately  $1 \times 10^6 \,\mathrm{J/m^3}$ . It is precisely due to its high kinetic energy that the CT can rapidly deposit into the core region of the plasma.

Figure 2(a) shown the temporal evolution of the EAST parameters during CT injection (t = 3.682 s), where it takes approximately 200 -  $400~\mu s$  for the CT to travel from triggering through the drift tube to reach the plasma boundary. After CT injection, the energy stored in EAST's plasma increased by 8 kJ, corresponding to a growth rate of approximately 16%—a change attributed to the energy brought by the CT injection. Concurrently, the line-averaged central density rose by roughly 30% following the injection. In addition to these changes in plasma energy and density, a rapid enhancement of the  $D_{\alpha}$  signal was observed as a direct response to the CT injection. Meanwhile, while the edge electron temperature decreased after the CT injection, the core electron temperature exhibited a significant increase at the same time.

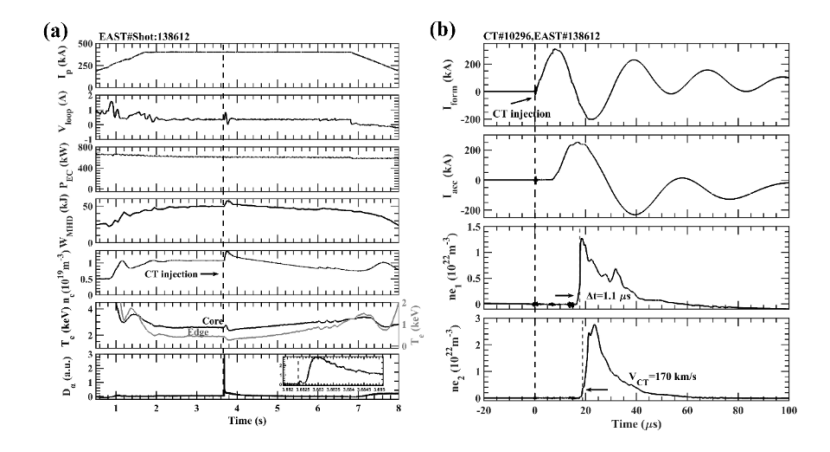


FIG. 2. Temporal evolution of EAST plasma parameters (shot:138612) during CT injection. (a) Plasma current, loop voltage, power of ECRH, plasma stored energy, central-line-averaged electron density, electron temperature, Da emission intensity. The discharge situation of the EAST-CTI system. (b) Formation current and acceleration current of CT, electron density measured at positions P1 and P2.

## 3.2 NONLOCAL CHARACTERISTICS OF PLASMA IN EAST TRIGGERED BY CT INJECTION

Figure 3 shows the evolution of core temperature following CT injection under different line-averaged densities  $(1.2 \times 10^{19} \, m^{-3} \,, \, 1.4 \times 10^{19} \, m^{-3} \,, \, 2.0 \times 10^{19} \, m^{-3})$  in EAST. After CT injection, the core temperature of the plasma shows different behaviors. As shown in figure 3(a) and 3(b), the core temperature increased sharply under low-density conditions, whereas figure 3(c) shows a sharp decrease in core temperature under high-density conditions. But compare figure 3(a) and 3(b), it can be seen that with the increase in density, the core temperature elevation is suppressed. This is because as the density increases, the perturbations induced by CT injection become relatively weaker, exerting a less significant influence on the density profile. Furthermore, this observation

suggests that the inversion phenomenon does not vanish abruptly with increasing density. Instead, it undergoes a gradual attenuation process.

As shown in figure 3(c), the temperature inversion disappears with further density increase. The temperature inversion phenomenon caused by cold pulse injection has a strong dependence on the density. Experimental studies conducted on the Alcator C-Mod tokamak indicate that the nonlocal effect can be

characterized by collisionality. Following a relationship expressed as  $v^* = \frac{v_{ei}}{\epsilon \omega_{be}} \propto \frac{qRZ_{eff}n_e}{T_e^2 \epsilon^{3/2}} \propto \overline{n}_e q_{95}R$  was able

to bring together observations from different tokamaks [29]. The magnitude of this threshold is related to the device's major radius R, average electron density  $\overline{n}_{\rm e}$  and boundary safety factor  $q_{95}$ . Here,  $v^*$  represents the collisionality. Among them, for  $q_{95} \sim 7$ , the values of  $v^*$  in these three discharges obtained were 15.9, 18.3 and 25.7 respectively.

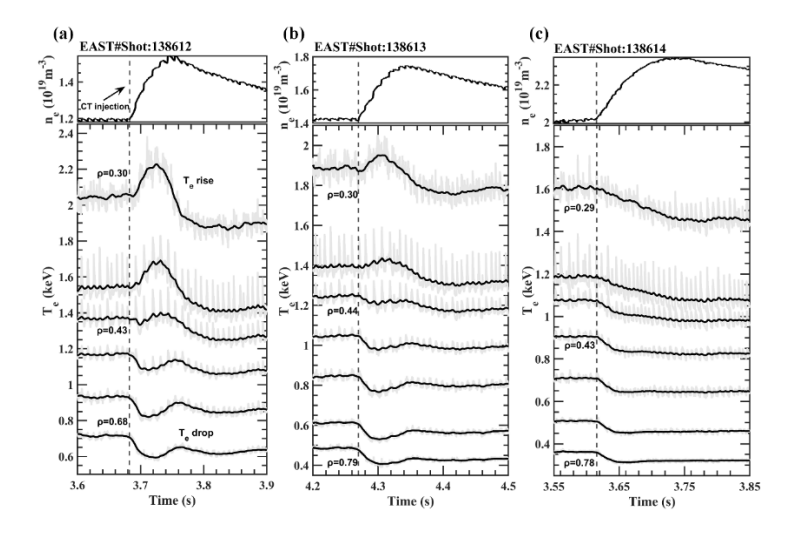


FIG. 3. The variation of electron temperature after CT injection under different line-averaged electron densities (from POINT interferometer). (a) low-density plasma (DN, ECRH,  $I_p$ =400 kA,  $\bar{n}_e$  = 1.2×10<sup>19</sup>  $m^{-3}$ ), (b) middle-density plasma (DN, ECRH,  $I_p$ =400 kA,  $\bar{n}_e$  = 2.0×10<sup>19</sup>  $m^{-3}$ ).

Figure 4 shows the evolution of relative variations in electron temperature and electron density at different radial positions during CT injection (t=3.682 s) in the low-density EAST discharge (EAST#138612). As shown in figure 4(a), the electron density relative variation evolution ( $(n_e - n_{e0}) / n_{e0}$ ,  $n_{e0}$  is the electron density at the time CT is on) reveals that, the electron density propagates from the edge to the plasma core on a very fast time scale after CT injection. The plasma core ( $\rho$ -0.17) begins to experience the arrival of the density pulse just 2 ms after injection, reaching a density peak at approximately 70 ms. And as shown in figure 4(b), illustrates the evolution of the relative variation in electron temperature ( $\Delta T_e$ ). The results show that core temperature of the plasma undergoes temperature inversion on a time scale almost the same as the core density and reaches the peak temperature at approximately 50 ms. In addition, during the temperature variation, a "mixing effect" was observed [16], characterized by a temperature trend of initial decrease followed by increase. It is noted that the peak of the temperature increase propagates outward gradually and diminishes progressively at  $\rho \sim 0.43$  to  $\rho \sim 0.68$ . Currently, no satisfactory explanation for this phenomenon exists.

As shown in figure 5(a), compared with the electron density profile at the moment of CT injection ( $t_0$ =3680 ms, black line), the electron density profile at 4 ms after CT injection (pink line) shows a certain increase in electron density at positions ( $\rho \sim 0.45$ ). This indicates that within the first 4 ms, the effect of CT injection on the density has already reached the position of  $\rho \sim 0.45$ . With 10 and 20 ms after CT injection (blue and green line), a significant increase in the electron density profile is evident at the core. This is due to the continuous inward diffusion caused by the CT injection. By comparing the evolution of the density profile during the initial stage of CT injection, it can be observed that CT injection causes the entire profile to flatten rapidly, this is crucial for inducing the core temperature inversion. Furthermore, figure 5(b) represents the evolution of electron temperature profiles during CT injection. Here, the black line represents the electron temperature profile at the moment of CT injection, while the blue line and red line denote the electron temperature profiles at 10 ms and 20 ms after CT injection, respectively. Comparison reveals that the temperature inversion occurs at  $\rho \sim 0.4$ -0.5. Compared with the

other fusion devices, the position of the temperature inversion surface is slightly different, which may be related to the plasma parameters and the size of the fusion device.

The evolution of core electron temperature ( $T_e$ ) is compared with normalized electron density gradient ( $a/L_{n_e}$ ) and normalized electron temperature gradient ( $a/L_{T_e}$ ) in figure 6. During the time period marked by the red box ( $t_1$ , approximately 3682 to 3686 ms), the core electron temperature changes gently, and the corresponding variation in the normalized electron temperature gradient is also small. However, the normalized electron density gradient at the core position shows rapid changes. This indicates that as the CT was introduced, the electron density gradient changed first, and the entire section rapidly became flatter. After entering the time period marked by the cyan box ( $t_2$ , approximately 3686 to 3727 ms), the core electron temperature continues to rise to a peak value. Correspondingly, the normalized temperature gradient first decreases continuously and then gradually recovers to near the horizontal line.

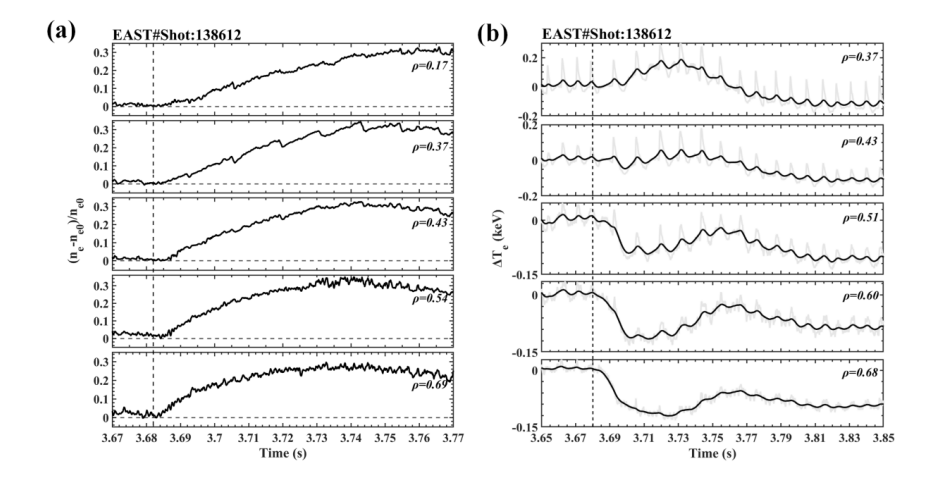


FIG. 4. Evolution of relative variations in electron temperature and electron density at different radial positions during CT injection.

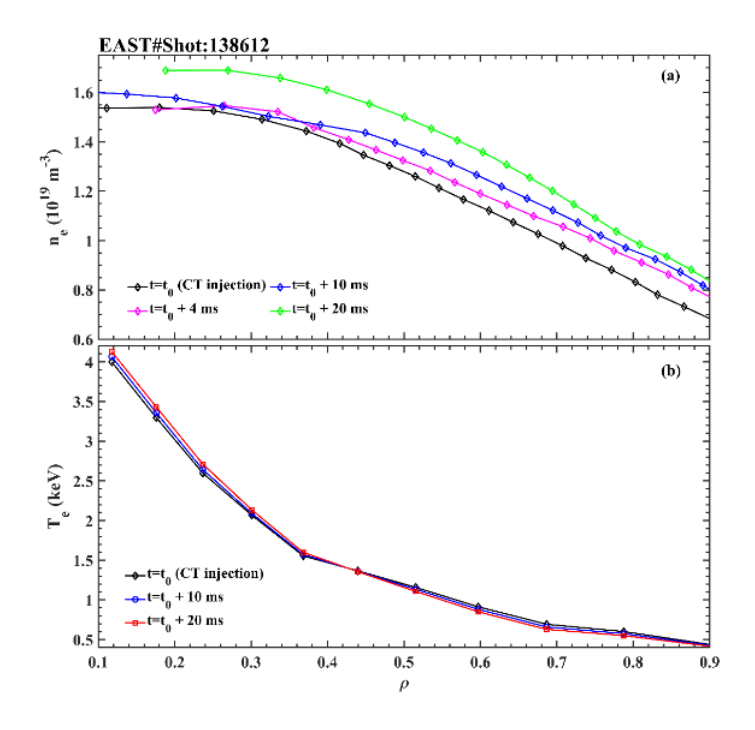


FIG. 5. The evolution of electron density profiles and electron temperature profiles after CT injection. (Black line represent the time of CT injection, Blue line represent 10 ms after CT injection, Red line represent 20 ms after CT injection.)

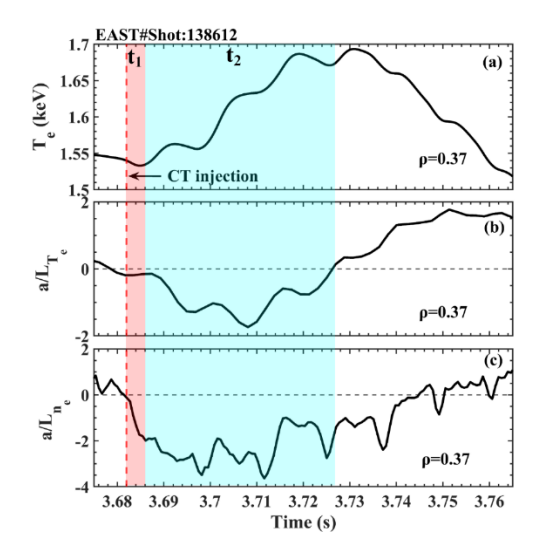


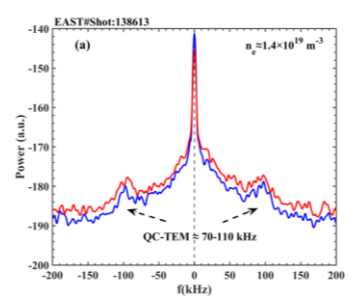
FIG. 6. The evolution of (a) core temperature  $T_e$ , (b) normalized temperature gradient  $a/L_{T_e}$  and (c) normalized ddensity gradient  $a/L_{T_e}$  after CT injection.

### 3.3 EXPERIMENTAL OBSERVATION OF QC-TEM AND MICRO-INSTABILITIES SIMULATIONS

Although it is challenging to distinguish between ITG modes and TEM via diagnostic measurements in experiments due to the overlap of their scale ranges. But a large body of existing experimental evidence indicates that the evolutionary behavior of the relevant turbulence can be determined by identifying the direct spectral characteristics of fluctuations induced by coherent mode instabilities [30-34]. As shown in figure 7, the spectral measurements of the plasma core obtained via the Doppler Backscattering system, there are two distinct symmetric peaks at the core position. These symmetric peaks correspond to the quasi-coherent-trapped electron mode (QC-TEM), whose association with the trapped electron mode (TEM) is widely recognized. A comparison of the spectral evolution characteristics before and after cold pulse (CT) injection indicates that the overall intensity of QC-TEM decreases to a certain extent after CT injection, suggesting that the TEM mode is stabilized after CT injection. The turbulence evolution features obtained from experiments will serve as crucial direct evidence for verifying the impact of turbulence on temperature inversion.

Noting that the core temperature reversal phenomenon is correlated with the evolution of plasma turbulence, we thus conducted numerical investigations on the turbulence characteristics of plasma before and after CT injection. This was achieved by leveraging the TGLF model in combination with previous experimental results [35-37]. The simulated input parameters include the electron temperature, electron density, ion temperature, heating power and the radial distribution of the safety factor. As shown in figure 8(a) the evolution of linear growth rate and the real frequencies before and after CT injection. Before CT injection, the core plasma ( $\rho = 0.18$ ) was dominated by the low-k TEM turbulence. This is consistent with the expectation that, under ECRH heating, the core plasma turbulence of EAST plasma is dominated by TEM. After CT injection, the growth rate of the lowk mode decreased significantly, which was the reason for the increase in the core temperature. This was precisely caused by the rapid flattening of the electron density profile resulting from the CT injection. And as shown in figure 8(b) there is no transition of turbulence modes from TEM-dominated to ITG-dominated. As depicted in figure 8(c) and (d), which present the growth rate and real frequencies at the plasma position of  $\rho = 0.62$ , the dominant mode remains the TEM. The difference is that there is no significant change in the growth rate before and after CT injection. Simulation results indicate that after CT injection, the low-k turbulence at the core of the plasma is stabilized, while the turbulence in the region outside the reversal surface remains unaffected by the CT injection. This simulation result is consistent with the suppression of QC-TEM observed in experiments.

The experimental results demonstrate that under the injection of CT, the electron density distribution flattens rapidly, and the TEM turbulence is effectively stabilized, which leads to a rapid increase in the core electron temperature. This phenomenon is fully consistent with the simulation results of the TGLF transport model.



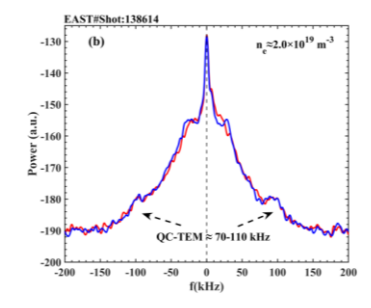


FIG. 7. Core plasma fluctuation spectra of EAST#138613 and EAST#138614 from the DBS system. The red line represents the spectra before CT injection, and the blue line represents that after CT injection.

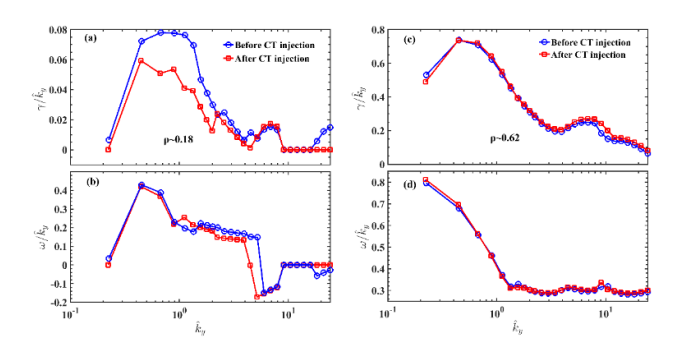


FIG. 8. Obtained through TGLF The linear growth rate (a) and (c), mode frequency (b) and (d) at  $\rho$ =0.18 and  $\rho$ =0.62. Blue line and the red line represent the situation before the injection of simulated CT and after the CT injection, respectively.

#### 4. DISCUSSION AND SUMMARY

Based on the characteristics of CT injection, this study conducted an experiment on core temperature inversion caused by cold pulse injection on EAST, expanding the understanding of non-local phenomena. In the experiment, core temperature inversion, disappearance of inversion under high density, and mixed effects were observed. The measurement using the reflectometer revealed an increase in the core electron density at 2 ms, which caused the electron density profile to flatten rapidly within an extremely short time. Furthermore, the time evolution analysis of the normalized electron density gradient, normalized electron temperature gradient, and core electron temperature during the CT injection process indicates that CT injection initially causes a rapid decrease in the normalized electron density gradient, followed by changes in the normalized electron temperature gradient and the core electron temperature. The spectra of plasma at the core is measured by DBS system, which revealed that QC-TEM is suppressed by CT injection. The changes in TEM intensity are generally considered to be consistent with those of QC-TEM intensity. The turbulent evolution characteristics obtained from the experiment are direct evidence of the influence of turbulence on the inversion. And the TGLF simulation also reached the same conclusion that the low-k turbulence in the core region of the plasma was suppressed after the CT injection. Based on the experimental and simulation results, it was found that the rapid injection of CT caused the density profile to flatten rapidly, thereby suppressing the TEM turbulence in the core and ultimately leading to a temperature inversion. The two key issues to be addressed in non-local phenomena—core temperature reversal and rapid temperature changes—are reasonably explained in this experiment. The mixing effects observed near the reversed surface require further investigation to verify their connection with the temperature reversal.

### **ACKNOWLEDGEMENTS**

This work was supported by the National MCF Energy R&D Program of China (Nos. 2024YFE03130001 and 2024YFE03130002), and the Institute of Energy, Hefei Comprehensive National Science Center (Anhui Energy Laboratory) (Nos. 21KZS202 and 23KHH140).

# REFERENCES

- [1] P. Rodriguez-Fernandez. et al 2017 Nucl. Fusion 57 074001
- [2] Gentle, K. W. et al 1995 Phys. Rev. Lett. 74 3620-3
- [3] Kissick M. W. et al 1996 Nucl. Fusion 36 1691-701
- [4] Zou X. L. et al 2000 Plasma Phys. Control. Fusion 42 1067-76
- [5] Ryter F. et al 2000 Nucl. Fusion 40 1917-32
- [6] Mantica P. et al 2002 Plasma Phys. Control. Fusion 44 2185-215
- [7] Sun H. J. et al 2010 Plasma Phys. Control. Fusion 52 045003
- [8] Liu Y. et al 2019 Nucl. Fusion 59 044005
- [9] Rice J. E. et al 2013 Nucl. Fusion 53 033004
- [10] Shi Y. J. et al 2017 Nucl. Fusion 57 066040
- [11] Shi Y.J. et al 2018 Nucl. Fusion 58 044002
- [12] Inagaki S. et al 2006 Plasma Phys. Control. Fusion 48 A251-7
- [13] Mantica P. et al 1999 Phys. Rev. Lett. 82 5048-51
- [14] del-Castillo-Negrete D. et al 2008 Nucl. Fusion 48 075009
- [15] Hariri F. et al 2016 Phys. Plasmas 23 052512
- [16] P. Rodriguez-Fernandez. et al 2018 Phys. Rev. Lett. 120 075001
- [17] P. Rodriguez-Fernandez. et al 2019 Phys. Plasmas 26 062503
- [18] Angioni C. et al 2019 Nucl. Fusion 59 106007
- [19] Li J. G. and Wang B. N. et al 2021 Engineering 7 1523-1528
- [20] Ye Y. et al 2025 Nucl. Fusion (accepted)
- [21] Liu X. et al 2014 Rev. Sci. Instrum. 85 093508
- [22] Qu H. et al 2015 Plasma Sci. Technol. 17 985
- [23] Liu H. Q. et al 2016 Rev. Sci. Instrum. 87 11D903
- [24] Hu J.Q. et al 2017 Rev. Sci. Instrum. 88 073504
- [25] Liu S. et al 2023 Rev. Sci. Instrum. 94 123507
- [26] Feng X. et al 2019 Rev. Sci. Instrum. 90 024704
- [27] Tan M. S. et al 2024 Fusion Eng. Des. 205 114559
- [28] Zhao Z. H. et al 2025 Plasma Sci. Technol. 27 065601
- [29] Gao C. et al 2014 Nucl. Fusion 54 083025
- [30] H. Arnichand. et al 2015 Nucl. Fusion 55 093021
- [31] H. Arnichand. et al 2016 Plasma Phys. Control. Fusion 58 014037
- [32] J. Citrin. et al 2017 Plasma Phys. Control. Fusion 59 064010
- [33] Zhong W. L. et al 2016 Phys. Plasmas 23 060702
- [34] H. Arnichand. et al 2014 Nucl. Fusion 54 123017
- [35] G. M. Staebler. et al 2007 Phys. Plasmas 14 055909
- [36] J. E. Kinsey. et al 2008 Phys. Plasmas 15 055908
- [37] Nan K.B. et al 2024 Plasma Phys. Control. Fusion 66 115015